In situ Raman Spectroscopy to Monitor Interfacial Electron Transfer Process: from Fundamental to Application Case Studies

Akiyoshi KUZUME, Ph.D.

Institute of Innovative Research, Tokyo Institute of Technology,
4259 Nagatsutacho, Midori-ku, Yokohama, 226-8503 Japan
Tel: +81-45-924-5873
E-mail: Kuzume.a.aa@m.titech.ac.jp

In situ Raman spectroscopy is capable of probing electron transfer processes under electrochemical condition by monitoring local structure and reactivity properties of solid/liquid interfaces. Therefore, *in situ* Raman spectroscopy is now recognized as one of the powerful surface characterisation techniques for the investigation of the fundamental and application studies, such as development of energy conversion and bio-mediating devices. In addition, an introduction of nanostructured surfaces increases the sensitivity of Raman signals, capable of observing spectroscopic features from molecular level. This article gives a brief history of Raman spectroscopy in the introduction, followed by an overview of the recent *in situ* Raman spectroscopic studies in our group, particularly focusing on the electrochemical and microbial electron transfer processes at solid/liquid interfaces under electrochemical condition.

Introduction

Raman effect, an inelastic scattering of light due to the excitation of vibrations, was first confirmed experimentally in 1923 and reported as "a new type of secondary radiation" in 1928 by Raman and Krishnan.[1] It was a significant discovery as a new spectroscopic principle as demonstrated later by the award of Nobel prize in Physics in 1930, only two years from its first publication. In general, a vibration that changes the polarisability (or simply the shape) of the target molecules by the irradiation is Raman active. However, the cross sections for Raman scattering is considerably small when compared with the Rayleigh band, which is typically about three orders of magnitude higher than the Stoke bands. Thus, the Raman spectroscopy at this early stage was not sensitive enough for detecting spectral feature at molecular scale due to the "excessive feebleness" of the effect. An intense illumination of laser can increase the Raman band intensity in general, but it heats up the sample during measurements, damaging surface species severely. Furthermore, fluorescence of the sample gives rise to the spectral background, which also limit the detection ability of Raman spectroscopy. In this way, one needs to wait nearly 50 years, until 1970s, for the renaissance of Raman spectroscopy.

The discovery of the surface enhanced Raman scattering (SERS) in 1973 (first reported by Fleischmann et al. in 1974[2]) for pyridine molecules adsorbed on an electrochemically roughened silver electrode surface stimulated the field of surface science since it demonstrated that the strong signal intensity of Raman bands can rival that of fluorescence, allowing the observation of single molecule on the surface. Later this experimental observation of SERS effect was explained by the subsequent publications in 1977 by Jeanmaire and Van Duyne[3] and Albrecht and Creighton,[4] proposing the enhancement mechanism of SERS based on electromagnetic and chemical effects, respectively. The former effect arises from the laser excitation of localised surface plasmon at roughen metal surface, while the latter effect comes from the charge transfer mechanism for adsorbed molecules with appropriate orbitals that interact with the metal substrate. These interpretations of the strong Raman enhancement on roughen surfaces triggers significant numbers of surface science investigations of SERS and opens up a great opportunity to explore not only solid surfaces but also electrochemical and biological (*in situ*) interfaces by designing highly sensitive surface observation techniques.

Further important progresses in SERS were made by the replacement of the electrochemically roughen surfaces with well-controlled nanostructured surfaces of both coinage and transition metals. Resulting from advances in

nanotechnology and improved instrumental capabilities, a fabrication of nanostructured surfaces for Raman substrate have been improved significantly during the last two decades. Precise design of the nanostructured surface in the dimension from 1 nm range are now possible via two approaches: A top-down physical approach and a colloidal-based bottom-up chemical approach. A top-down approach refers to slicing or successive cutting of a bulk material to get nano-sized particle. A bottom-up approach, on the other hand, refers to the building material from the bottom atom by atom, molecule by molecule or cluster by cluster. Particularly with the nanostructures in the size range between 10 and 100 nm, a specific surface plasmon resonance property appears to give pronounced enhancement effect on Raman signals of molecules on and nearby the surface. Since the SERS intensity strongly depends on the excitation wavelength and the strength of the surface plasmons propagating on the surface of the metal nanoparticles, it is important to adjust the surface plasmon resonances by tuning the size, shape, chemical composition and configurations (such as alloy and core-shell) of nano-surfaces to obtain reproducible Raman data, allowing not only a qualitative but also a quantitative analysis. Many reviews and book chapters are available for learning further development of SERS in detail.[5]

A recent development in electrochemistry has focused predominantly on the characterisation of the solid/liquid interface to understand the local electron transfer reactions and the effect of surface structures on the reactivity in the molecular level. Since late 1980s, the interfacial electrochemistry underwent a significant progress by the introduction of well-defined Clavilier-type single crystal surfaces as a major breakthrough.[6] This progress led to other new surface technologies such as microscopic and spectroscopic techniques, as well as theoretical simulations. In particular, *in situ* spectroscopic techniques, such as surface enhanced Raman and infrared spectroscopy, allow monitoring simultaneously the electrochemical reactivity and structural changes of the redox-active species vicinal to the electrode surface.[7] By combining electrochemistry with *in situ* microscopic and spectroscopic approaches, the underlying fundamentals of the electron transfer (ET) processes at solid/liquid interfaces under electrochemical condition have been increasingly well understood in the last two decades.

Here in this article, some recent *in situ* Raman spectroscopic investigations studied in our group are described in the field of fundamental surface science towards application in the development of energy conversion catalysts and bio-mediating devices. Along with this line, I would like to emphasise that the combination of surface electrochemical characterisation tools at the nanoscale range with complicated materials such as 3D metal complex films and microbiological system offers unique opportunities for the emerging field of *in situ* investigation to explore processes and interactions at the solid/liquid interfaces.

Experimental

All *in situ* Raman measurements were performed using a LabRAM HR800 confocal microscope (Horiba Jobin Yvon) (Figure 1A). The 800 mm focal length monochromator allows characterisation of subtle samples with high sensitivity and high spatial resolution. A long working distance objective lens (50 times magnification: LMPLFLN from Olympus) was employed with a numerical aperture of 0.5 in order to focus either a diode-pumped solid state (DPSS) laser or a He-Ne laser beams (excitation wavelength of 532 and 632.8 nm, respectively) at typical laser power around 3 - 6 mW on the sample. The Raman signal was collected in a back-scattering geometry. We used a home-made spectro-electrochemical Kel-F cell for *in situ* measurements which is equipped with a Pt wire and an Ag/AgCl electrode as counter and reference electrodes, respectively, together with inlet and outlet of gas and solution flux, allowing to exchange the solution/gas during spectroscopic measurements without disturbing its optical configuration (Figure 1B).

Cyclic voltammetry (CV) is a popular technique for initial electrochemical studies to obtain information about complicated electrode reaction. It involves sweeping the electrode potential between two potential values at a certain scan rate consecutively in both direction, thus “cycling

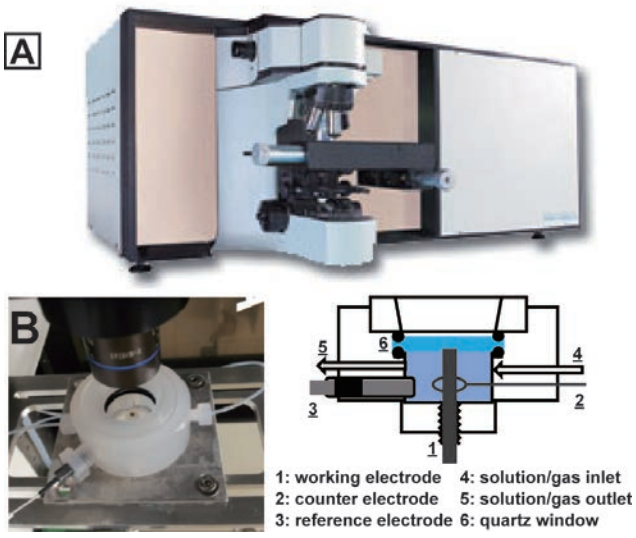

Figure 1 (A) a LabRAM HR800 confocal microscope and (B) a home-made Kel-F spectro-electrochemical cell.

electrode potentials". The current value is recorded as a function of the applied potential and plotted as a cyclic voltammogram.

In situ Raman Spectroscopy Case Study

CO oxidation on Pt(100)

Electrochemical CO adsorption and oxidation reaction on Pt surfaces is one of the most important and fundamental interfacial studies in the electrocatalysis of small organic molecules. CO, at the same time, acts as a poison of Pt anode catalysts in the proton exchange membrane fuel cell, and thus, electrochemical CO adsorption and oxidation on single crystal Pt electodes as a model studies, as well as on size- and shape-controlled Pt nanoparticles, have been investigated in detail, revealing a strong correlation between surface structure and catalytic activity. A Langmuir-Hinshelwood type of reaction mechanism was proposed for the CO oxidation, which is based on the reaction of adsorbed CO molecules with adsorbed oxygen-containing species (often assigned to adsorbed OH formed by the oxidative chemisorption of water molecules on Pt). Typical cyclic voltammograms of CO oxidation on Pt surface in 0.1M H_2SO_4 shows two oxidation peaks, a prepeak followed by a main stripping peak, indicating the CO oxidation process proceeds in two steps (Figure 2). The main peak is assigned to the oxidation of adsorbed CO on terrace sites accompanied with the formation of oxygen-containing species. On the other hand, the assignment of the prepeak is proposed to be a CO oxidation at active sites, such as steps and defects. The position and the magnitude of the prepeak depend on crystallographic orientation, type and density of defects, CO coverage, as well as surface pretreatment. The prepeak is particularly pronounced for high coverage CO on well-ordered Pt(100)-(1×1) electrode than those with other morphology,

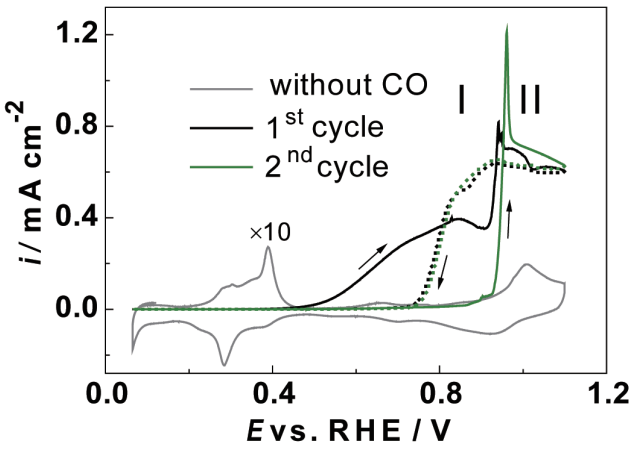

Figure 2 The first (black) and second (green) voltammetric cycles of CO electro-oxidation in CO-saturated 0.1M H_2SO_4 on Pt(100). The solid and dotted lines represent the anodic and the corresponding cathodic potential scans. (Reproduced with permission from ref. 8. Copyright 2014, Elsevier Ltd.)

although it disappears in the subsequent second potential cycles. The mechanism and the cause of the pronounced prepeak on Pt(100) surface, as well as the disappearance in the second cycle, were not clarified so far. We combined *in situ* approaches, i.e. scanning tunnelling microscopy (STM) and *in situ* Raman spectroscopy, with single crystal electrochemistry to interpret the nature of the interfacial processes (structure change, activity, adsorption/desorption etc.) of CO prepeak under operating condition.[8]

Shell-isolated nanoparticle enhanced Raman spectroscopy (SHINERS) method was introduced in this study to monitor Raman signal of CO molecules adsorbed on atomically flat Pt(100) surface. Normally, the experimental requirements of SERS measurements are the use of roughen or nanostructured surfaces, composed of coinage substrate materials. SHINERS is one of the advanced SERS technique,[9] using Au nanoparticles that are covered by 2-3 nm thick silica shell as an optical antenna (or authors called it "smart dust"), which are spread on the flat surface. Smart dusts enhance Raman signals of molecules on and near their surface, but would not interact chemically nor electrically with the molecules due to the presence of silica shell. In this way, one can use any flat surfaces, no need of coinage substrate, and further, one can ignore the chemical and electric interaction between the optical antenna and substances. In this study, CO does not adsorb on Au nanoparticles, but only on Pt(100) surface, thus Raman signals observed are only from adsorbed CO on Pt(100) surfaces.

Figure 3A, 3D show a series of *in situ* Raman spectra of adsorbed CO on Pt(100) surfaces, showing Raman bands at 477-484, 1869-1877 and 2054-2080 cm^{-1} which were assigned to an on-top Pt-CO stretching ($\nu(Pt\text{-}CO_L)$), two-fold-bridging CO stretching ($\nu(CO_B)$) and on-top CO stretching ($\nu(CO_L)$) modes, respectively. The broad shoulder around 407 cm^{-1} is assigned to the Pt-CO stretching mode on bridge sites ($\nu(Pt\text{-}CO_B)$). Observations of both bridge and on-top modes represent typical spectroscopic signatures of the compressed CO dense monolayer on the surface, as observed in *in situ* STM experiments. Figure 3 summarised the potential dependencies of Raman shift and normalised integrated intensities of the CO_L-related bands as recorded in the first anodic, cathodic and the subsequent second anodic scans. In the lower potential range, two bands show distinct linear shifts of the peak position until the onset of the prepeak around 0.4 V, while the corresponding intensities remain constant. It is followed by the changes in frequency trend at higher potential (E > 0.5 V) indicating the notable decrease of the dipole coupling interaction with neighbouring CO, while the simultaneous decrease in the intensity reflects a

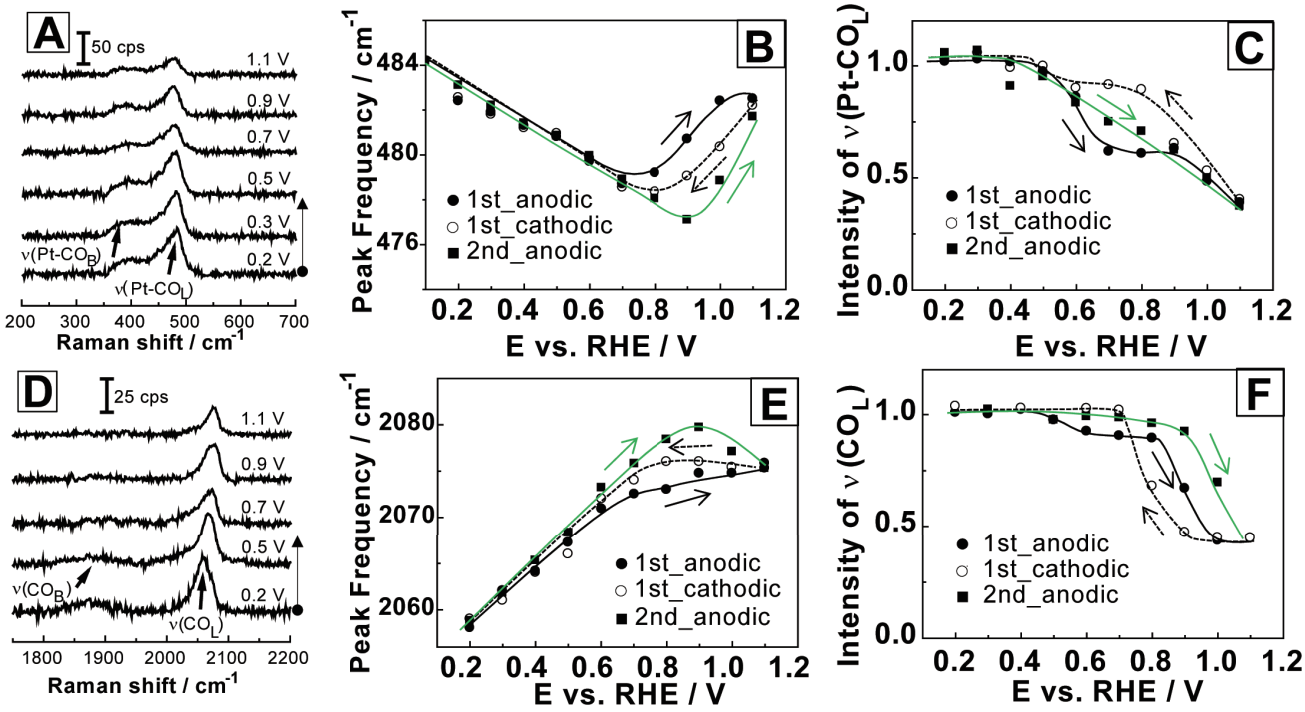

Figure 3 Potential dependent steady-state SHINER spectra of the CO adlayer on a Pt(100) in CO-saturated 0.1M H_2SO_4 for the first anodic scan (A, D), and Raman frequency shifts (B, E) and integrated intensities (C, F) of $\nu(Pt\text{-}CO_L)$ (A-C), and $\nu(CO_L)$ (D-F) modes in dependence on the applied potentials. (Reproduced with permission from ref. 8. Copyright 2014, Elsevier Ltd.)

decrease of the CO coverage on the Pt surface. Both trend evolve at potential higher than the onset of the prepeak process. *In situ* STM experiments demonstrated the structure changes of the substrate starts at E = 0.83 V.[8] Increasing the potential towards more positive values, such as 0.86 V leads to the nucleation and growth process of Pt adatoms, pulled out from the surface at the edges of the large Pt islands with monatomic height. It is important to point out that the onset of prepeak takes place at 0.4 V, where no structure change was observed in STM measurements, strongly indicating that the appearance of the prepeak is not caused by the defect sites formed by the potential increase as proposed by some authors in literatures.

A distinctly different evolution of the Raman spectra was revealed during the second potential cycling: There is no display of a CO prepeak in CV (Figure 2). We found that the electrochemical response in the first anodic scan can be reproduced after the second cycle if CO is removed completely from the solution and electrode surface, and subsequently being readsorbed at 0.1 V on a hydrogen terminated Pt surface. In addition, dosing of CO in the potential region of anion adsorption leads to a significant reduction in magnitude of the prepeak. Those observation contradict with some literatures that the "irreversible degradation" of the Pt(100) surface with small Pt adatoms led to the loss of the prepeak feature, which cannot explain the recovery of the Pt(100) prepeak features after complete CO removal and subsequent redosing.

Attempts to propose an alternative mechanism of Pt(100) deactivation/reactivation in the prepeak region require to consider the active centre as well as the role of adsorbed CO as reactant and blocking species. Deactivation may be caused by the vanishing of the specific active sites, where need to be accessible for the co-adsorption of CO and oxygen-containing species. Therefore, the alternative reason for the deactivation of Pt(100) surface might be that the potentially active sites are blocked by CO preventing the formation/coadsorption of oxygen-containing species which hinders the subsequent oxidation of CO.

Based on the combination of the observation in CV, *in situ* microscopic and spectroscopic studies, we rationalised the deactivation of the prepeak feature in the CO oxidation reaction on Pt(100) surfaces. When CO was dosed at 0.1 V on a hydrogen-terminated Pt(100) surface, there seems to be still a small amount of specific sites where hydrogen is not replaced by CO adlayer (adsorbed monolayer). These adsorbed hydrogens are oxidatively desorbed at E > 0.4 V, where the specific sites are competitively occupied by oxygen-containing species, CO and anion. The oxygen-containing species interact with neighbouring CO molecules leading to the electro-oxidation of the latter. These particular sites are activated for the CO oxidation in the prepeak potential range. Increasing the potential to E > 0.9 V triggers the electro-oxidation of bulk CO on terrace sites. In the subsequent cathodic scan, the CO molecules cover the entire surface, including the specific sites above mentioned, hindering

the co-adsorption of oxygen-containing species. Thus, the CO prepeak is suppressed in the second anodic scan.

We have performed single crystal voltammetric experiments in combination with morphological studies employing *in situ* STM and *in situ* SHINERS studies, successfully demonstrating the electro-oxidation reactivity characteristics during potential cyclings.

CO_2 reduction on SnO_2 electrocatalysts

The growing carbon dioxide (CO_2) content in the atmosphere and additional anthropogenic activity, such as burning of fossil fuels and the destruction of forests, has captured noticeable attention by scientists in the past century due to the significant effects on the global climate. Numbers of technologies on the capture and the sequestration of CO_2 have been developed to decrease the level of CO_2 content in the air. Among those, a number of literatures and reports dealing with the electrochemical reduction of CO_2, in particular, is rising ever since it was first described by the pioneering work of Royer in 1870.[10] The electrochemical reduction of CO_2 involves multiple proton-coupled electron transfer steps, yielding CO, formate, hydrocarbons (CH_4, C_2H_4, C_2H_6) and alcohols (CH_3OH, C_2H_5OH, 1-Propanol) in aqueous media at room temperature. In the 1980's, Hori et al. reported significant features of electrochemical reduction of CO_2 at metal electrodes, rationalising the product selectivity with the electrode materials.[11] Authors roughly categorised the metals into two groups on the basis of CO_2 conversion products; one mainly forms CO (Cu, Au, Ag, Pt, Pd, Zn, Ni and Ga) and the other forms formate (Hg, Pb, Tl, Cd, In, Sn). Among those metals, tin have attracted considerable attention due to their high activity towards formate production and its rather low cost compare to platinum-group and coinage metals. In general for Sn/SnO_x catalyst system, the overall effect of product selectivity and reaction efficiency depends on many experimental conditions, such as its morphology, chemical and oxidation state, temperature, CO_2 pressure/concentration, overpotentials and the pH of the electrolyte. In this way, the reported values of a faradaic efficiency (FE) of formate production from electro-reduction of CO_2 shows wide discrepancies in literatures: in a range between 5 to 90%.

Detail characterisation of catalyst properties under reaction condition is necessary for understanding its catalytic properties: reactivity, selectivity and stability in the long-term electrolysis process. However, it is still a great challenge to monitor simultaneous dynamic changes in the structural and chemical properties of heterogeneous nanostructured catalyst *during* the electrolysis in the real electrolysis cell. *Operando* Raman spectroscopy*1, in this context, is a promising technique that can provide a real-time chemical information of nanostructured catalyst properties, allowing us to establish correlations between structure, activity, stability and its selectivity towards CO_2 electro-reduction.

*1: *Operando* Raman spectroscopy: Raman spectroscopic characterisation of catalysts under realistic reaction conditions with simultaneous real-time online analysis of reaction products

In order to observe chemical changes of a real SnO_2 catalyst under the reaction condition, *operando* Raman spectroscopic studies were carried out using reduced graphene oxide (rGO) supported SnO_2 nanoparticles (SnO_2 NPs) as an electro-catalysts for the electrolysis of CO_2 reduction in aqueous solution with different pH values.[12] Previous studies in literatures revealed that the stability of tin oxides depends heavily both on the pH and the applied electrode potential.[13] Therefore, measurements were carried out with slightly or heavily alkaline solution in the pH range between 8.5 and 12, which were prepared by controlling CO_2 bubbling time through a 0.5 M NaOH solution until the desired pH was achieved.

A series of potential dependent steady state Raman spectra shows three distinctive Raman signals at 478, 628 and 770 cm^{-1} due to E_g, A_{1g} and B_{2g} modes in all electrolyte solutions (Figure 4A). In the same potential range for catalytic reaction of CO_2 reduction, SnO_2 itself could also be reduced to metallic Sn. Therefore, it is highly challenging to separate the true catalytic current for CO_2 reduction on SnO_2 apart from the overlapped parallel degradative reduction current of SnO_2 itself to metallic Sn. To visualise latter contents, the integrated intensity of the main peak at 628 cm^{-1} was plotted against electrode potentials for pH 8.5, 9.7 and 12.0, respectively (Figure 4B). Three potential regions labeled I to III can be distinguished as (I) the region of native SnO_2 phase; (II) the intermediate region where SnO_2 are partially (20-25%) reduced to metallic Sn and (III) the region after complete reduction of SnO_2 to metallic Sn. The conversion from region I to II took place around -0.5 V in the pH 8.5 solution, while it appeared at -0.7 V in solutions at pH 9.7 and 12.0. The normalised intensity values in the region II are around 75-80% of that of region I and shows the intensity plateau down to $E < -1.2$ V.

By combining product analysis using gas and ion-exchange chromatographies, formate and CO concentration, together with the faradaic efficiency (FE) values for formate production, were obtained as a function of potential and pH of the solution (Figure 4C). By comparing the measured FE values (production selectivity of SnO_2) with the results of Raman spectroscopy (degradation of SnO_2),

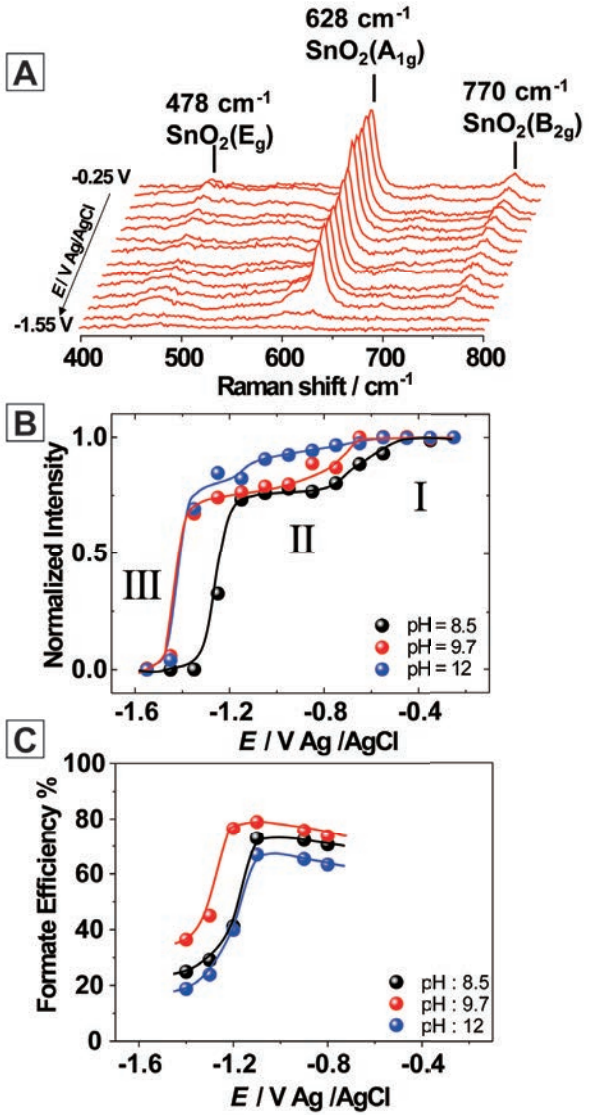

Figure 4 Potential dependent *operando* Raman study at varied potential and pH. (A) potential dependent Raman spectra at pH 9.7, (B) the relative intensity of A_{1g} Raman peak and (C) the FE values as a function of applied potentials. (Redrawn plots from the data in ref 12 with permission of Copyright 2015 American Chemical Society)

FE of formate production shows a strong dependence on the oxidation state of the catalyst surface. At moderately cathodic potentials, the FE is increasing with decreasing electrode potentials, however at more negative range, this tendency breaks and the FE curves go over a maximum. At very negative potentials, where catalysts are completely reduced to metallic Sn, the FE for the formate production and the intensity of A_{1g} peaks are both heavily decreased. Interestingly, the maxima of the FE curves are at such potentials where the thermodynamically stable phase should be metallic Sn (determined based on the Pourbaix diagram[13b]). However, the reduction of the SnO_2 NPs is kinetically hindered, and thus, the Raman peak is still of considerable intensity, indicating that the catalyst is only partially reduced and the SnO_2 phase is still prevalent. This conclusion clearly reveals that the presence of surface oxide plays significant roles in the catalytic activity to form formate during CO_2 electro-reduction on tin electrodes. Finally, we have demonstrated clear feasibility of *operando* Raman spectroscopic studies under operating conditions. A careful combination of surface detection tools at nanoscales with commercial applications allows us exploring the emerging field of CO_2 research and energy development.

Extracellular Electron Transfer process at interface between microbes and metal electrode

The discovery of electrogenic bacteria has been a big breakthrough in the research of new energy technologies paving the way for the development of microbial electrochemical technology (MET), such as microbial fuel cells, microbial electrosynthesis, microbial water desalination cells, and microbial electro-remediating cells for restoring polluted environments. The fundamental understanding of the interfacial processes taking place between individual electrogenic bacteria and an electrode is proposed to be dominated by the outer membrane cytochromes (OMCs), which are located at the outermost cellular membrane near the electrode surface. Therefore, it is important to establish an efficient electric communication between the microorganisms and the electrode via OMCs, lowing the interfacial resistance, thus leading to the overall higher current production or higher performance of microorganisms in the MET.

The electrogenic bacteria, *Geobacter sulfurreducens* (*Gs*), which produce the highest current densities of known pure cultures, represent the most thoroughly investigated family of electrogenic bacteria. OMCs on the *Gs* surface was proposed to be responsible for the direct electron transfer (ET) to the metal electrodes, a process that actually fails if the amount of OMCs is strongly reduced. Since the role of the OMCs in the direct heterogeneous ET is far from being understood, it is important to explore the simultaneous monitoring of the electrochemical response and of structural changes of OMCs for understanding the complex nature of ET processes and interactions involved in whole-cell studies under operating condition.

Recently, in this context, we have studied the electrochemical activity and structural properties of *Gs* cells directly adsorbed on bare gold electrodes using a combination of *in situ* spectroscopic, microscopic and electrochemical methods.[14-16] Our strategy combines single crystal electrochemistry with *in situ* atomic force microscopy (AFM) to characterise the morphology of *Gs* submonolyers, with surface-enhanced infrared absorption spectroscopy (SEIRAS) and gap-mode surface enhanced Raman spectroscopy (GM-SERS) to access *in situ* molecular information of the *Gs*/electrode interfaces with high

surface selectivity and sensitivity.

A submonolayer (subML) of *Gs* was prepared using the electrostatic adsorption of the bacteria cells, which bear a negative surface charge, on positively charged Au(111) and Ag(111) electrodes in a bicarbonate buffer solution containing 20 mM acetate (works as an electron donor), previously deoxygenated with N_2: CO_2 (4:1) mixed gas. These conditions ensure that *Gs* cells adsorb in their stable oxidised form. The morphology of the bacterial adlayer as obtained after 12 hours of polarisation was characterised by scanning electron microscopy (SEM) and *in situ* AFM. Both confirmed the presence of a subML of rather isolated, homogeneously distributed microbial cells firmly attached to the electrode surface. The average population of *Gs* cells amounts to 10 ± 2 cells per 100 μm^2, which translates into a coverage of 10%. The formation of the subML ensures that the further *in situ* investigation focuses only on the ET at the bacteria/electrode interface, and not at the bacteria/bacteria interfaces. The redox-activity of the immobilised microbial subML of *Gs* cells on Au(111) was investigated by CV (Figure 5A). A direct electrochemical detection of the redox signals in the CV indicated clearly that some domains of the outermost microbial surface were close enough to the electrode to undergo ET across the interface. The electrochemical response reached a steady state after five cycles accompanied by a considerable decrease of the redox current in the entire potential region. The corresponding voltammogram is characterised by two pairs of peaks with mid-points potentials at -0.12 and -0.33 V (inset of Figure 5A). These electrochemical behaviours at a steady state indicates a slow, surface-confined redox process, the redox potential of which are in the same range as those previously reported in the extracellular c-type cytochrome OmcZ.[17]

Similar to the CV experiments, a steady state spectroscopic response is reached after five cycles in attenuated total reflection (ATR)-SEIRA spectra, which shows a reversible, potential dependent behaviour. By decreasing potential values, the evolution of the amide I signal at 1686 cm^{-1} was observed accompanied by an increase in the intensity of the interfacial water bending and stretching modes during the cathodic scan.[14] The amide I and water bands decreased during the subsequent anodic scan. These experimental observations reveal the following important aspects: (i) the reversible evolution of the steady state SEIRA spectra upon potential cycling between the reduction and oxidation forms of *Gs* cells suggests that the coverage of *Gs* cells does not change during the potential cycling, (ii) the microbial cells retain the direct electrical communication to the metal electrode, (iii) the significant potential-dependent shift of the amide I band from 1659 cm^{-1} (oxidized state) to 1686 cm^{-1} (reduced state) suggests a secondary structure change of redox active proteins from α-helix to β-turn. It was proposed that the electrical field-induced conformation transition in the protein structure may lead to a more favourable configuration for the interfacial electron exchange.

The structure properties of the heme centres in the outer membrane cytochrome C units, such as OmcZ, are directly accessible during the interfacial ET under electrochemical control by using *in situ* GM-SERS. GM-SERS employed 55 nm diameter silver nanoparticles (Ag NPs) as plasmonic antenna, which were mixed with *Gs* solution and subsequently drop-cast at subML coverage (ca. 10%) on a smooth Ag electrode. The combination of Ag NP and Ag surface enables the choice of a green excitation laser (wavelength of 532 nm), which tails with the plasmonic resonance of the NPs as well as with the Q-band of the heme centres. Figure 5B shows the GM-SERS response of a subML of *Gs* in their oxidised

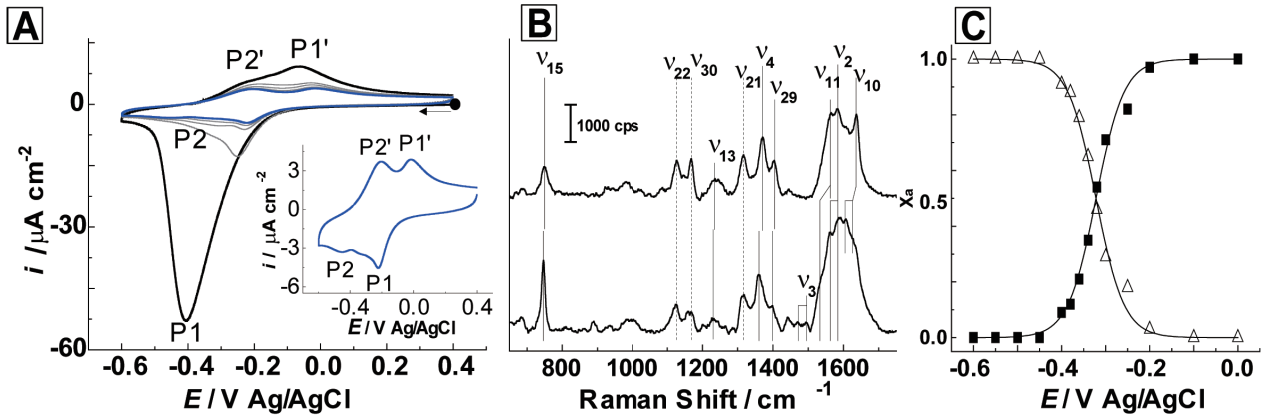

Figure 5 (A) Cyclic voltammograms of the *Gs* subML on Au(111) at a scan rate of 0.01 Vs^{-1}. Black line: cycle 1, Grey lines: cycles 2 to 7. Inset: CV of the corresponding cycle 8 (blue). (B) Potential dependent GM-SER spectra of a *Gs* subML mixed with Ag NPs in the oxidised state at 0.0 V (upper) and the reduced state at -0.6 V (lower), respectively. The spectra were obtained with the excitation at λ = 532 nm (laser power at 1 mW with 150 mm defocussed, acquisition time of 10 s); (C) potential dependent molar fraction (X_a) of the oxidised (full square) and the reduced (empty triangle) form derived from the component analysis of the ν15 band in the experimental GM-SER spectra. The solid lines represent fits of the Nernst equation for a one-electron redox couple. (Redrawn plots from the data in ref 14 with permission of Copyright 2014 the Owner Societies).

(0.0 V) and reduced (-0.6 V) forms. Although it is difficult to make an unambiguous assignment of individual bands due to the broad features, the spectra revealed distinguishable bands from c-type cytochromes in the oxidised forms by comparing with a normal Raman spectra of the solid *Gs* samples. For the oxidised *Gs* cells, the position of the spin-state marker bands ν2 and ν10 indicated a six-coordinated low-spin state of the heme with a histidine and a methionine group as axial ligands. This result suggested that the OMCs retain mostly their native structure at the positively polarised electrode/electrolyte interface upon constant laser radiation. Our Raman experiments also demonstrated that the presence of the Ag NPs does not seem to interfere with the active functionality of the surface-confined *Gs* cells, although one cannot exclude a possibility of the partial internalisation of silver NPs.

Potential excursion towards negative values leads to the electrochemical reduction of the *Gs*, which is accompanied by distinct changes in the simultaneously recorded Raman spectra. Clear downshifts in wavenumber and a splitting of the spin marker states were observed for ν2, ν4, ν10, ν11 and ν15 modes. The two strong bands ν4 and ν15 are particularly sensitive to the redox state of the heme protein. Both represent symmetric ring breathing modes of the pyrrole moiety, which is N-coordinated to the Fe-centre. The integrated intensity of the redox marker band ν15 was quantitatively analysed as a function of the applied electrode potential to monitor the spectroscopic redox response of the adsorbed microbial cells. The molar fraction of oxidised and reduced forms show a clear S-shaped behaviour (Figure 5C). Simulating this redox process within the *Gs* subML by the superposition of the component spectra allows estimating the relative concentrations of the two redox states as a function of the applied electrode potential. A fit of the Nernst equation leads to an effective redox potential at -0.32 V and an effective number of exchanged electrons of 0.8. The former value is in good agreement with the range of the *Gs*-related redox potentials as derived from CV experiments, while the latter value is lower than the expected value for the redox process of a c-type cytochrome of uniform nature. This result suggests a certain distribution of interfacial redox potentials, which is in good agreement with the multiple peak voltammetric profiles. It is noteworthy that the splitting of the spin-marker modes ν2, ν3 and ν10 upon transformation of coexistence of a low spin and a high spin state. The nature of this transition is not yet clear.

As a consequence, we have presented clear evidences that OMCs in close contact with metal electrode changes their structures and electrochemical properties with the electrode potential at the bacteria/electrode interface by utilising *in situ* spectroscopic techniques. This interfacial effect decrease with increasing the distance between the bacteria and electrode surface by introducing self-assembled monolayer (SAM).[15] Furthermore, we modified Au electrode with SAM of ω-functionalised alkyl-thiols containing different outer linking groups, where bacteria were immobilised, to investigate the linker effect on the biocompatibility of the SAM and the current production properties of *Gs* cells.[16] In particular, the carboxyl-anchoring group provides biocompatible conditions for the OMCs of the *Gs*, which facilitate the heterogeneous ET at the microorganism/electrode interface. Our surface-electrochemistry based approach on the subML of microbial cells demonstrates the feasibility of exploring the single cell *in situ* investigation under operating condition. The combination of surface electrochemical tools at the nano- and micro-scale with microbiological approaches offers unique opportunities for the emerging field of electro-microbiology to explore processes and interactions between microorganisms and electrical devices.

Conclusion

It was briefly overviewed the history of Raman spectroscopy followed by the recent *in situ* Raman spectroscopic studies in our group, particularly focussing on the electrochemical and microbial electron transfer processes at the solid/liquid interfaces under electrochemical condition. Since the discovery of the first report on the surface-enhanced Raman scattering in 1974, along with the technical improvement in the instruments, surface-enhanced Raman spectroscopy has been developed into a powerful surface diagnostic technique in the investigation of the fundamental and application studies. *In situ* Raman spectroscopy using a LabRAM HR800 confocal microscope is now capable of probing electron transfer processes in molecular level under electrochemical condition by monitoring the local structure and the activity properties of solid/liquid interfaces.

References

[1] C.V. Raman, K.S. Krishnan, Nature 121, 501 (1928).

[2] M. Fleischmann, P.L. Hendra, A.J. McQuillan, Chem. Phys. Lett. 26, 163 (1974).

[3] D.L. Jeanmaire, R.P. Van Duyne, J. Electroanal. Chem. 84, 1 (1977).

[4] M.G. Albrecht, J.A. Creighton, J. Am. Chem. Soc. 99, 5215 (1977).

[5] Just for examples, (a) S. Schluecker, Angew. Chem. Int. Ed. 53, 4756 (2014); (b) Z.Q. Tian, B. Ren, D.Y. Wu, J. Phys. Chem. B 37, 9463 (2002); (c) S. Schluecker "Surface Enhanced Raman Spectroscopy" Wiley-VCH, Weinheim (2011); (d) R. Aroca "Surface-Enhanced Vibrational Spectroscopy" Wiley, West Sussex (2006).

[6] J. Clavilier, D. Armand, S.G. Sun, M. Petit, J. Electroanal. Chem. 205, 267 (1986).

[7] (a) Z.Q. Tian, B. Ren, Annu. Rev. Phys. Chem. 55, 197 (2004); (b) D.Y. Wu, J.F. Li, B. Ren, Z.Q. Tian, Chem. Soc. Rev. 37, 1025 (2008).

[8] A.V. Rudnev, A. Kuzume, Y. Fu, Th. Wandlowski, Electrochim. Acta 133, 132 (2014).

[9] J.F. Li, Z.Q. Tian et al. Nature 464, 392 (2010).

[10] M.E. Royer Compt. Rend. Hebd. Séances Acad. Sci. 70, 731 (1870).

[11] Y. Hori, H. Wakebe, T. Tsukamoto, O. Koga, Electrochim. Acta 39, 1833 (1994).

[12] A. Dutta, A. Kuzume, M. Rahaman, S. Vesztergom, P. Broekmann, ACS Catalysis 5, 7498 (2015).

[13] (a) S. Lee, H.K. Ju, R. Machunda, S. Uhm, J.K. Lee, H.J. Lee. J. Lee, J. Mater. Chem. A 3, 3029 (2015); (b) M. Pourbaix, Atlas d'equilibres electrochimique; Gauthier-Villars et Cie: Paris, P 479 (1963).

[14] A. Kuzume, U. Zhumaev, J. Li, Y. Fu, M. Füeg, M. Estévez, Z. Borjas, Th. Wandlowski, A. Esteve-Nuñez, Phys. Chem. Chem. Phys. 16, 22229 (2014).

[15] M. Füeg, Z. Borjas, M. Estévez, A. Esteve-Nuñez, I.V. Pobelov, P. Broekmann, Th. Wandlowski, A. Kuzume, *submitted to* Bioelectrochemistry.

[16] A. Kuzume, U. Zhumaev, J. Li, Y. Fu, M. Füeg, M. Estévez, Z. Borjas, A. Esteve-Nuñez, Th. Wandlowski, Electrochim. Acta 112, 933 (2013).

[17] (a) K. Inoue, X. Qian, L. Morgado, B.C. Kim, T. Mester, M. Izallalen, C.A. Salgueiro, D.R. Lovley, Appl. Environ. Microbiol. 76, 3999 (2010); (b) K. Inoue, C. Leang, A.E. Franks, T.L. Woodard, K.P. Nevin, D.R. Lovley, Environ. Microbiol. Rep. 3, 211 (2011).